ELSEVIER

Contents lists available at ScienceDirect

Pharmacological Research

journal homepage: www.elsevier.com/locate/yphrs





Targeting of the IGFBP3/TMEM219 pathway restores intestinal stem cells capability of healing mucosa in gastrointestinal autoimmune disorders*

Giovanni Amabile ^{a,1}, Francesca D'Addio ^{b,c,1}, Anna Maestroni ^b, Monique Zangarini ^a, Stefano Porzio ^a, Maria Gabriella Camboni ^a, Emma Assi ^b, Adriana Petrazzuolo ^b, Cristian Loretelli ^b, Moufida Ben Nasr ^{b,d}, Vera Usuelli ^b, Ahmed Abdelsalam ^b, Andy Joe Seelam ^{b,d}, Monica Zocchi ^b, Domenico Corradi ^e, Virna Marin ^a, Chiara Bruckmann ^a, Marta Nardini ^a, Filippo Canducci ^a, Claudia Nardini ^a, Silvio Danese ^f, Gianvincenzo Zuccotti ^g, Gianluca M. Sampietro ^h, Sandro Ardizzone ⁱ, Paolo Fiorina ^{b,c,d,*}

ARTICLE INFO

Keywords: TMEM219 IGFBP3 Monoclonal antibodies Intestinal organoids

ABSTRACT

Insulin-like growth factor binding protein 3 (IGFBP3) signals through the death receptor TMEM219 to modulate survival of target cells; inhibition of this signaling has been associated with a rescue of intestinal stem cell death. Here we report the screening, generation, and characterization of fully human IgG monoclonal antibodies (mAbs) through phage display or by hybridoma technology, that block IGFBP3 or TMEM219. Both anti-IGFBP3 and anti-TMEM219 mAbs showed high affinity binding with the target antigens and potent effects in protecting selfrenewal ability of intestinal stem cells in in vitro relevant assays. Among all the mAbs tested, anti-TMEM219 mAbs generated by phage display, particularly Ent001, showed the highest score in displacing the IGFBP3/ TMEM219 binding and in rescuing intestinal stem cells (ISC) markers expression and function in IGFBP3cultured human mini-guts obtained from healthy donors. In human in vitro proof-of-concept studies, in which we generated mini-guts from patients with immune-mediated intestinal disease such as Crohn's disease, Ent001 successfully restored mini-guts growth and ISC markers' expression, while expression of the proapoptotic IGFBP3-related factor Caspase 8 was downregulated. In vivo, in models of DSS-induced chronic colitis and in inflammatory-mediated carcinogenesis, Ent001 significantly improved disease activity index and histological score, restored mucosal morphology and abrogated the development of carcinomas, leading to mucosal healing. In summary, Ent001 represents a novel IGFBP3/TMEM219 inhibitor to be further tested and developed in clinical studies as a novel therapeutic in immune-mediated and inflammatory intestinal diseases.

^a Enthera, Milan, Italy

b International Center for T1D, Pediatric Clinical Research Center Romeo ed Enrica Invernizzi, Department of Biomedical and Clinical Sciences Università di Milano, Milan. Italy

^c Division of Endocrinology, ASST Fatebenefratelli Sacco, Milan, Italy

^d Transplantation Research Center, Brigham and Women's Hospital, Harvard Medical School, Boston, MA, USA

e Department of Medicine and Surgery, Unit of Pathology, University of Parma, Parma, Italy

f Gastroenterology and Endoscopy, IRCCS Ospedale San Raffaele and Medicine and Surgery Department, Vita-Salute San Raffaele University, Milan, Italy

g Pediatric Clinical Research Center Romeo ed Enrica Invernizzi-Università di Milano and Buzzi Children's Hospital, Milan, Italy

^h Division of General and HBP Surgery, Rho Memorial Hospital, ASST Rhodense, Milano, Italy

i Gastrointestinal Unit, ASST-Fatebenefratelli Sacco, Milan, Italy

^{*} This article is co-authored by an associate editor. According to our policy the article has been handled by another editor independently, with the authors being blind to the whole process.

^{*} Correspondence to: Nephrology Division, Boston Children's Hospital, Harvard Medical School, Boston, MA, USA. *E-mail address*: paolo.fiorina@childrens.harvard.edu (P. Fiorina).

¹ These authors equally contributed to the work

1. Introduction

Insulin-like growth factor binding-protein 3 (IGFBP3) circulates in blood bound to Insulin-like growth factor 1 (IGF-1) and acts as a carrier and regulator of the IGF-1 availability, thereby ensuring the control of critical physiological processes like cell survival, differentiation and proliferation [1–4]. In the last decade, a novel role for IGFBP3 as a proapoptotic factor acting in an IGF-1 independent manner has rapidly emerged [5–9]. Studies conducted *in vitro* and in preclinical models demonstrated that IGFBP3 mediates cell death/apoptosis by binding to an IGFBP3 receptor [10], further identified as TMEM219, which is a death factor acting through the activation of the Caspase 8 cascade [1,6,11]. In particular, IGFBP3 targets TMEM219-expressing cells in certain cells and tissues [12], particularly the endodermic-derived intestine and pancreas [13–15]. *In vitro* and *in vivo* studies also showed that a

disruption of the IGFBP3/TMEM219 axis exists in disease conditions such as diabetic enteropathy and autoimmune diabetes, with IGFBP3 being significantly altered and able to deliver a death signal into the target cells [14,15]. More importantly, abrogation of this IGFBP3-mediated detrimental effects in intestinal stem cells (ISCs) as well as in insulin-producing beta cells through the use of the recombinant protein ecto-TMEM219, prevented cell damage, thereby reducing the extent of intestinal disorders and of diabetes [14,15]. Based on these premises, we have generated and tested in *in vitro* relevant assays and in strategic *in vivo* preclinical models, therapeutic monoclonal antibodies (mAbs) capable of blocking IGFBP3 and TMEM219 in the context of immune-mediated intestinal diseases to identify a clinical candidate to be evaluated in future studies. We ultimately demonstrated that blockade of the IGFBP3/TMEM219 axis with the selected mAbs has a beneficial effect both *in vitro* and *in vivo* in rewiring the intestinal

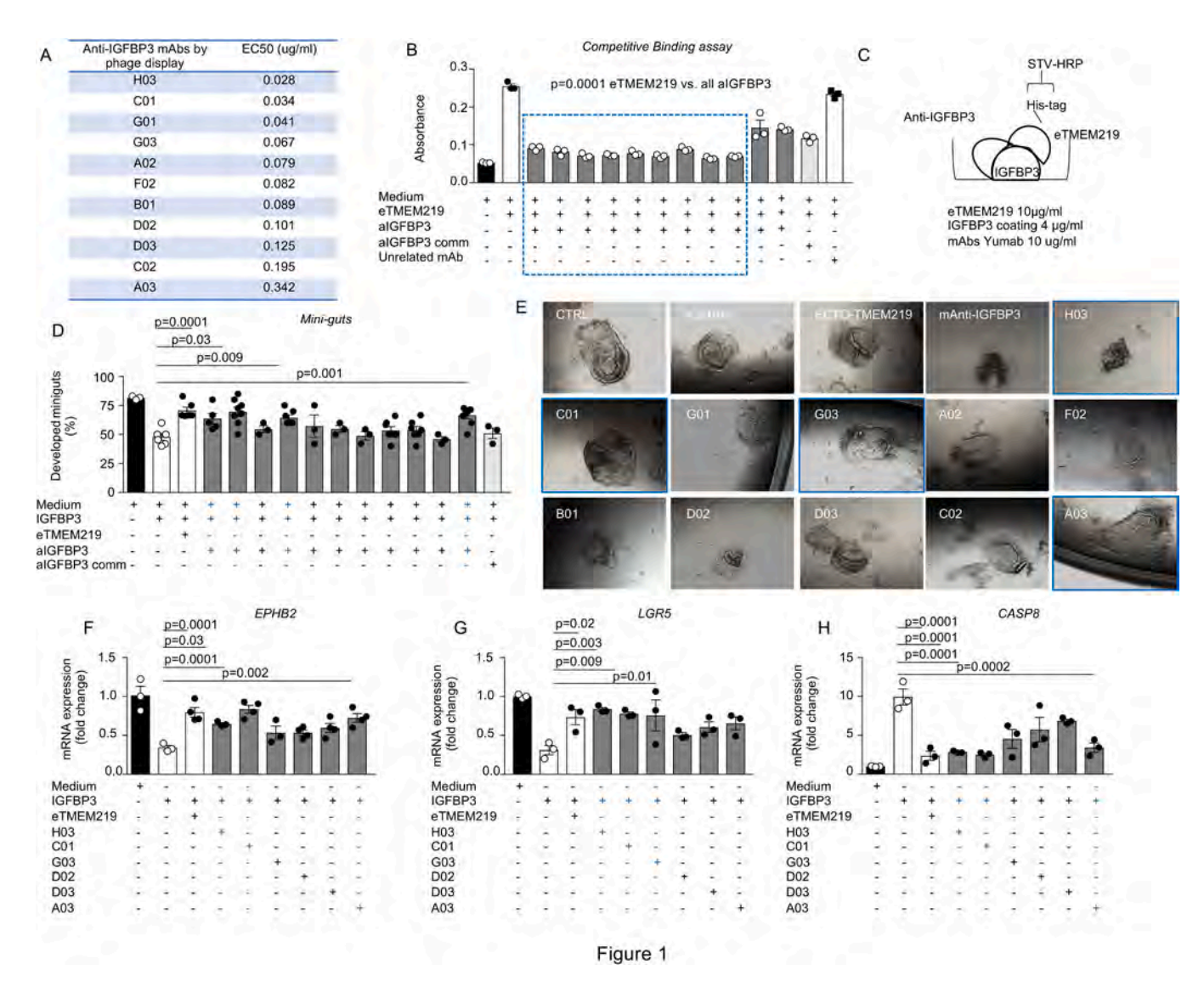


Fig. 1. Generation of anti-IGFBP3 mAbs by phage display and characterization of their activity. (A). List of anti-IGFBP3 mAbs generated by phage display with their half maximal effective concentration (EC50). (B, C). Bar graph quantifying the ability of anti-IGFBP3 mAbs to bind IGFBP3 and displace the extracellular portion of TMEM219 (eTMEM219). The blue square highlights the mAbs blocking the IGFBP3/TMEM219 binding with the higher rate. In C the schematic representation of the competitive ELISA binding assay employed in B. Absorbance signal of ecto-TMEM219 was measured. (D, E). Bar graph quantifying the percentage of developed miniguts obtained from crypts of healthy subjects and cultured for 8 days with/without IGFBP3 (50 ng/ml) and with anti-IGFBP3 mAbs. Commercial anti-IGFBP3 mAb (Novus Biological) and ecto-TMEM219 were used as controls. In E pictures showing morphology of developed mini-guts with blue squares highlighting the anti-IGFBP3 mAbs with better effect. Original magnification 10X. (F, G, H). Bar graphs showing relative mRNA expression of EPHB2 (F), LGR5 (G) and CASP8 (H) quantified by qRT-PCR in mini-guts cultured with/without IGFBP3 and with/without anti-IGFBP3 mAbs. In blue mAbs with statistically significant effect are highlighted. Data are expressed as mean ± standard error of the mean (SEM). mRNA expression was normalized to ACTB. Abbreviations: CASP8, Caspase 8; mAb, monoclonal antibody; eTMEM219, newly generated recombinant protein based on TMEM219 extracellular portion.

mucosal healing ability in the context of immune-mediated inflammatory injuries, thus paving the way for the development of a novel therapeutic in intestinal human diseases.

2. Results

2.1. Generation of anti-IGFBP3 mAbs by phage display and characterization of their activity

We first selected IGFBP3 as antigen of interest and generated human anti-IGFBP3 mAbs, which specifically target the IGFBP3 binding to the extracellular portion of the IGFBP3-receptor TMEM219, by using two different approaches, the phage display and the hybridoma-based technology (Supplementary Fig. 1A-B). The first approach generated 11 humanized anti-IGFBP3 mAbs, the second approach generated 10 affinity-matured human mAbs, the latter from two different clones obtained from two different library screening (n = 1 from the first and n = 9 from the second library screening). All the 11 anti-IGFBP3 mAbs produced by phage display showed good binding with the IGFBP3 antigen and an EC50 ranging between 0.028 and 0.342 µg/ml (Fig. 1A). Furthermore, a competitive ELISA, in which the capability of inhibiting the IGFBP3-TMEM219 binding was tested, demonstrated that 9 out of 11 mAbs had a more potent effect as compared to the commercially available anti-IGFBP3 mAb (p < 0.0001), and were further selected for in vitro biological assays (Fig. 1B-C). An epitope binning analysis also demonstrated that all newly generated anti-IGFBP3 mAbs were able to bind to IGFBP3 in presence of the anti-IGFBP3 commercial antibody (from Novus Biologic), thus suggesting that the binding region was different and supporting the novelty of the generated mAbs. The ability of the newly generated anti-IGFBP3 mAbs in preventing apoptosis/death of target cells was tested in vitro in crypts organoids (i.e., mini-guts). Mini-guts were generated from crypts obtained from healthy subjects and cultured for 8 days upon IGFBP3 exposure and in the presence/ absence of newly generated anti-IGFBP3 mAbs. Among the 11 mAbs generated by phage display, 4 out of 11 (C01, A03, G03, and H03) successfully rescued the self-renewal ability and morphology of large crypt organoids in the presence of IGFBP3 (C01: p = 0.0001, G03: p = 0.03, H03: p = 0.009 and A03: p = 0.001, vs. IGFBP3), with an increase of fully developed mini-guts by at least 20 % (Fig. 1D-E). Furthermore, all 4 mAbs, which were effective in abrogating the IGFBP3 negative effect on mini-guts, also obtained an upregulation of the ISC markers EPHB2 and LGR5 and a downregulation of the pro-apoptotic IGFBP3-related marker CASP8, with the mAbs C01 and H03 showing the most powerful effect (p = 0.0001 vs. IGFBP3, Fig. 1F-H). Our findings demonstrate that anti-IGFBP3 mAbs generated by phage display are effective in blocking the IGFBP3/TMEM219 binding and in rescuing the IGFBP3-mediated damage in intestinal cells.

2.2. Generation of hybridoma-based anti-IGFBP3 mAbs and characterization of their activity

By using the hybridoma-based technology, we next generated other 10 anti-IGFBP3 mAbs, which were all able to bind IGFBP3 with high affinity (KD <10 $^{-12}$), with 9 out of 10 exhibiting also a strong effect in blocking the IGFBP3/TMEM219 binding *in vitro* in a competitive ELISA assay and being thus tested *in vitro* biological assays (Supplementary Fig. 2A-B). First, we demonstrated that 3 out of 10 mAbs (M1, E08 and E20) improved the development of min-guts cultured in the presence of IGFBP3, with a 20 % increase as compared to commercial mAbs (anti-IGFBP3 Novus biological), which did not obtain any significant effect (Supplementary Fig. 2 C). Moreover, addition of the M1 and E08 mAbs to mini-guts culture in the presence of IGFBP3 also re-established the expression of the ISC markers *EPHB2* and *LGR5* and downregulated that of *CASP8*, whose dysregulation in the presence of IGFBP3 in this assay has been already described (Supplementary Fig. 2D-F) [15]. These observations demonstrate that anti-IGFBP3 mAbs generated by hybridoma

are effective in rescuing the self-renewal ability of the mini-guts but to a lesser extent as compared to anti-IGFBP3 mAbs generated by phage display (Table 1).

2.3. Generation of anti-TMEM219 mAbs by phage display and characterization of their activity

To further implement the therapeutic armamentarium able to target the IGFBP3/TMEM219 signaling, we next moved to generate mAbs able to couple with the IGFBP3 receptor TMEM219. We employed the same approaches as above and produced 5 humanized anti-TMEM219 mAbs by phage display (Fig. 2) and 8 anti-TMEM219 by hybridoma-based technology (Supplementary Fig. 3). All 5 anti-TMEM219 mAbs generated by phage display showed binding with the extracellular portion of TMEM219 used to test the binding affinity and a KD $< 2 \times 10^{-8}$ M (p = 0.0001 vs. ectoTMEM219, Fig. 2A-C). To address whether blockade of the receptor was also able to obtain a biological effect, we tested the newly generated anti-TMEM219 in the mini-guts assay. Mini-guts generated from crypts obtained from human healthy donors were cultured for 8 days upon IGFBP3 exposure and in the presence/absence of anti-TMEM219 mAbs (50 ng/ml and 10 μ g/ml respectively) and a commercial polyclonal rabbit anti-human TMEM219 antibody was also included as a control antibody. First, we demonstrated that among the 5 newly generated phage display anti-TMEM219 mAbs that were most effective in blocking the IGFBP3/TMEM219 binding, TC01, TC02 (p = 0.0001 vs. IGFBP3) and TE01 but to a less extent (p = 0.01 vs.)IGFBP3), were able to rescue mini-guts growth up to 75 % upon IGFBP3 exposure (Fig. 2D). This was associated with an increased mRNA expression of EPHB2 and LGR5 and a decrease in the CASP8 mRNA expression, particularly when TC01 was added (mean fold change: 2.5 vs. 5, p = 0.03) as compared to TC02 and TE01 (p = ns, Fig. 2E-G). These findings demonstrated that targeting the IGFBP3 receptor TMEM219 was also successful in protecting intestinal self-renewal abilities and in halting IGFBP3-mediated cell damaging.

2.4. Generation of hybridoma-based anti-TMEM219 mAbs and characterization of their activity

Eight anti-TMEM219 mAbs were generated by the hybridoma technology and showed high affinity to the extracellular portion of TMEM219, with a KD $< 10^{-12}$ M (Supplementary Fig. 3 A). While all the anti-TMEM219 mAbs generated were able to block the binding between TMEM219 and IGFBP3 in a competitive ELISA with a statistically significant difference, 3 out of 8 showed the most potent effect in displacing the IGFBP3/TMEM219 interaction (Supplementary Fig. 3B-C). The 3 anti-TMEM219 mAbs were selected for in vitro testing in the mini-guts assay, with TM1 and TE04 being able to rescue the self-renewal ability of mini-guts in the presence of IGFBP3 (p = 0.0001 and p = 0.02respectively, Supplementary Fig. 3D). Moreover, TM1 partially restored the expression of the ISC marker LGR5, while a slight effect was obtained on EPHB2, with CASP8 mRNA expression being downregulated with both TM1 and TE04 (p = 0.0003 and p = 0.0004 respectively, Supplementary Fig. 3E-G). These findings demonstrate that the anti-TMEM219 mAbs generated by the hybridoma-based technology were able to nearnormalize the IGFBP3-mediated detrimental effects in vitro in the minigut assay, although to a lesser extent as compared to anti-TMEM219 mAbs generated by phage display (Table 1). These observations further suggest that the potential clinical candidate to inhibit the IGFBP3/TMEM219 signaling in human studies may be selected among phage display generated anti-TMEM219 mAbs.

2.5. In vitro proof-of-concept human studies and selection of clinical candidate

To finally prove the efficacy of the newly generated anti-TMEM219 mAbs in a highly clinically relevant setting, we next tested the anti-

Table 1
Summary score of anti-IGFBP3 and anti-TMEM219 mAbs generated by phage display and hybridoma technology in *in vitro* testing.

	aIGFBP3 phage display	aIGFBP3	hybridoma	aTMEM219 pl	hage display	aTMEM2	19 hybridoma
Displacement axis	4	3		5		4	
In vitro mini-guts	3	3		4		2	
ISCs marker	5	4		5		5	
Effect on CASP8	5	5		4		4	
Total score	17	15		18		15	
Scoring system: 0–5							
Score		0	1	2	3	4	5
Displacement axis		Increase of binding	No displacement	Up to 25 %	Up to 50 %	Up to 75 %	> 75 %
In vitro mini-guts healthy vs. IGFBP3: Ratio IGFBP3/treatment		Decreased grown	Ratio = 1	Ratio up to 1.2	Ratio up to 1.3	Ratio up to 1.5	Ratio > 1.5
ISCs marker vs. positive control and IGFBP3		Reduced	No change	Improvement low	moderate	medium	high
Effect on CASP8 vs. positive control		Increased	No change	Reduction low	moderate	medium	high

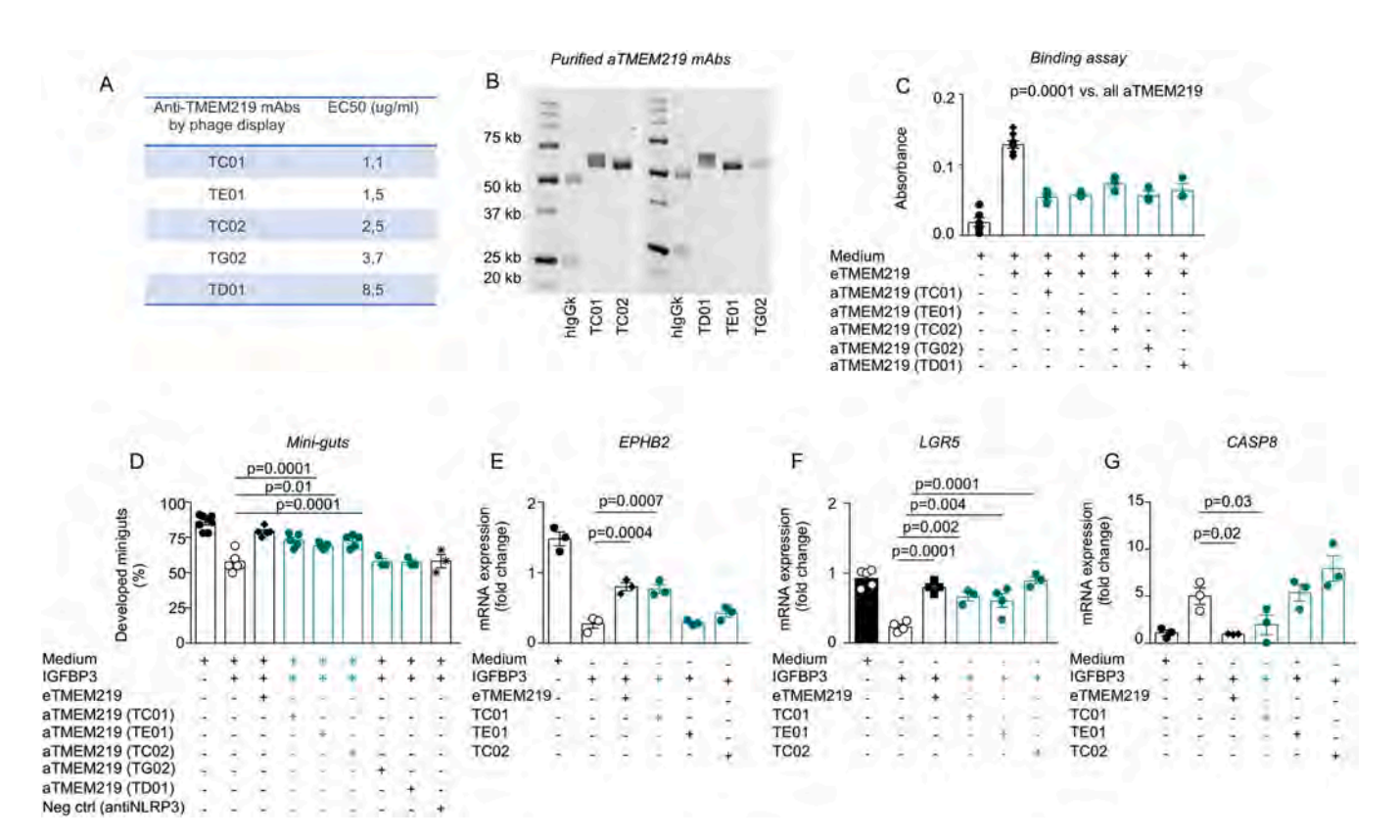


Fig. 2. Generation of anti-TMEM219 mAbs by phage display and characterization of their activity. (A, B). List of anti-TMEM219 mAbs generated by phage display with their half maximal effective concentration (EC50) and SDS-PAGE showing newly generated purified anti-TMEM219 mAbs. (C). Bar graph quantifying the ability of anti-TMEM219 mAbs to bind eTMEM219 and displace the binding with IGFBP3. Absorbance signal of ecto-TMEM219 was measured. (D). Bar graph quantifying the percentage of developed mini-guts obtained from crypts of healthy subjects and cultured for 8 days with/without IGFBP3 (50 ng/ml) and with anti-TMEM219 mAbs. eTMEM219 was used as positive control. (E, F, G). Bar graphs showing relative mRNA expression of EPHB2 (E), LGR5 (F) and CASP8 (E) quantified by qRT-PCR in mini-guts cultured with/without IGFBP3 and with/without anti-TMEM219 mAbs. In green mAbs with statistically significant effect are highlighted. Data are expressed as mean ± standard error of the mean (SEM). mRNA expression was normalized to ACTB. Abbreviations: CASP8, Caspase 8; mAb, monoclonal antibody; eTMEM219, newly generated recombinant protein based on TMEM219 extracellular portion.

TMEM219 mAb, which showed the best performance in our in vitro assays, TC01, namely Ent001, in mini-guts generated from crypts of patients with long-established inflammatory bowel disease (IBD). Indeed, to better highlight the relevance of targeting our IGFBP3/TMEM219 axis in an immune-mediated intestinal disease such as IBD, we employed two different models. In the first one, we analyzed the development of normal self-renewing crypts organoids generated from crypts of patients with long-term Crohn's disease (n = 5 with history of disease > 5 years) cultured in the presence of IGFBP3 and with Ent001. Addition of Ent001 improved the grown of Crohn's derived mini-guts in the presence of IGFBP3, with a 25 % increase and paralleling that observed in mini-guts developed from healthy subjects (mean \pm SEM: $72.6 \pm 3.2 \%$ vs. $56.7 \pm 4.3 \%$, p = 0.001, Fig. 3A-B). This was

associated with a recovered mRNA expression of the ISC markers *EPHB2* and *LGR5* (Fig. 3C-D) and a decrease in the mRNA expression of the proapoptotic IGFBP3-mediated signaling marker *CASP8* (Fig. 3E). Interestingly, the detrimental effect of other factors such as high glucose (35 mM), which modestly reduced organoids growth, was not rescued by TMEM219 inhibition (mean 72 % vs. 69 % with high glucose, p = ns), thereby confirming the selectivity for the IGFBP3/TMEM219 signal. In a second set of experiments, we tested the effect of Ent001 in mini-guts generated from crypts of healthy subjects and cultured with pooled serum of patients with Crohn's disease (at least 5 donors, 10 % in place of regular FBS), which is associated with increased expression/activation of TMEM219 signaling [16]. Indeed, mini-guts cultured in Crohn's disease serum developed less and showed a spheroid

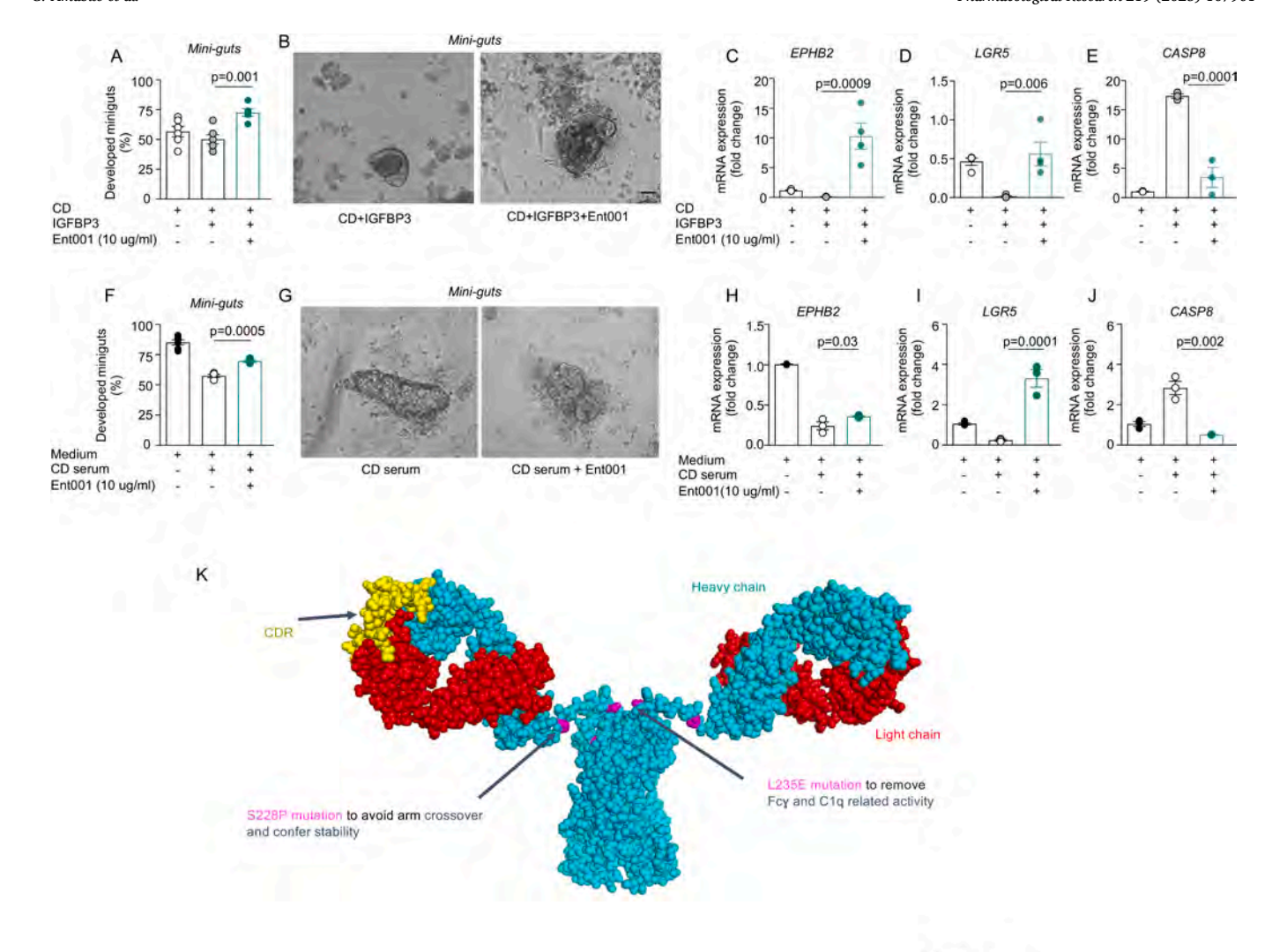


Fig. 3. *In vitro* proof-of-concept human studies and selection of clinical candidate. (A, B). Bar graphs and pictures showing mini-guts obtained from crypts of patients with Crohn's disease and cultured with/without IGFBP3 and in the presence/absence of anti-TMEM219 Ent001. Original magnification 20X. (C, D, E). Bar graphs depicting normalized expression (fold change) of *EPHB2* (C), *LGR5* (D) and *CASP8* (E) quantified by qRT-PCR in mini-guts obtained from crypts of Crohn's disease patients and cultured with/without IGFBP3 and in the presence/absence of anti-TMEM219 Ent001. (F, G). Bar graphs and pictures depicting mini-guts obtained from crypts of non-IBD patients and cultured in the presence of 10 % pooled sera of patients with Crohn's disease in place of FBS and with/without anti-TMEM219 Ent001. Original magnification 20X. (H, I, J). Bar graphs showing normalized expression (fold change) of *EPHB2* (H), *LGR5* (I) and *CASP8* (J) quantified by qRT-PCR in miniguts obtained as reported in F-G. (K). 3D representation of the clinical candidate Ent001, anti-TMEM219 mAb, generated by phage display. Sites of mutation are highlighted in the figure in violet. In yellow the binding site of extracellular TMEM219. Data are expressed as mean ± standard error of the mean (SEM). mRNA expression was normalized to *ACTB*. Abbreviations: CD, Crohn's disease patients; CASP8, Caspase 8.

morphology, thereby mimicking those grown from patients with Crohn's disease (Fig. 3F-G). More importantly, Ent001 was able to near-normalize the development and morphology of crypts organoids cultured with Crohn's disease serum (57 \pm 2.6 vs. 70 \pm 1.7, p = 0.0005 vs. Crohn's disease serum) and this was associated with an upregulation of the ISC markers EPHB2 and LGR5, and with a downregulation of CASP8 (Fig. 3F-J). This data confirmed the ability of Ent001 in preserving the self-renewal ability of intestinal crypts also in intestinal disease conditions, thus emphasizing the potential clinical relevance that it may have in future studies. In order to proceed with this monoclonal antibody as clinical candidate we performed a final characterization of the compound, which included also the 3D modelling of the mAb that has been generated and the identification of the binding site to the TMEM219 protein. In particular, a 3D structure of Ent001 was designed through a bioinformatic tool and modelled based on the structure of a neutralizing human full-IgG, in which both Fc and Fab portions were identified, and the CDR region was highlighted as the binder region for TMEM219 (Fig. 3K). Positions of mutations introduced to stabilize the structure and avoid cytotoxicity and complement activation were also pinpointed. In summary, Ent001 was delineated as the lead clinical candidate to target the IGFBP3/TMEM219 signaling in intestinal immune-mediated human diseases.

Figure 3

2.6. The anti-TMEM219 mAb Ent001 improves DSS-induced chronic colitis in vivo

To finally determine the relevance of targeting the IGFBP3/TMEM219 axis *in vivo* in relevant preclinical models, we tested the newly generated anti-TMEM219 mAb Ent001 in a chronic colitis treatment model, in which Dextran sulfate sodium (DSS) was given in three repeated oral cycles at 2 %. Mice received the anti-TMEM219 mAb Ent001 intraperitoneally daily from day 18 to day 32, and then twice a week until day 42. A remarkable decrease in the disease activity index (DAI) score, associated with a decrease in weight loss and an increased

colon size, was demonstrated in animals developing chronic colitis and treated with Ent001 (p = 0.0001, Fig. 4A-C). This observation was paralleled by an improvement of the histological score in animals receiving DSS+ Ent001 (Fig. 4D) and with a reduction in T cell infiltration, both CD3 and CD4 cells, at the immunostaining, with crypts and mucosa morphology being fully rewired (Fig. 4E-G). A notable decrease in the proinflammatory cytokines MIP1beta, KC, IFN-gamma, IL-12p40 and G-CSF was also evident in DSS+Ent001-treated animals, while IL-22 serum level, low in mice receiving DSS and shown to have a protective effect on intestinal homeostasis, was near-normalized with Ent001 (Supplementary Fig. 4A-F). Expression of CXCL10, IL-6 and CCL25 mRNA was also downregulated in the intestinal specimens of mice receiving DSS + Ent001 as compared to DSS-treated animals, further confirming that Ent001 counteracted the development of inflammatory-

mediated signs and symptoms of colitis (Supplementary Fig. 4G-I). Finally, an RNA sequencing analysis conducted on flow-sorted intestinal cell subsets including Epcam⁺CD44^{hi}CD24^{low} intestinal stem cells, Epcam⁺ enterocytes, enteroendocrine cells, intestinal absorptive and secreting progenitors and Tufts cells, demonstrated a significant upregulation of proinflammatory factors in all the cell populations analyzed and obtained from mice developing chronic colitis and treated with vehicle as compared to naïve untreated animals (Fig. 4H-J). Expression of those proinflammatory markers, which were mainly linked to leukocytes recruitment and chemotaxis (Fig. 4K), was fully abrogated in all intestinal cell subsets of mice with chronic colitis and treated with Ent001. Interestingly, *Sprr2d* and *IL-1b* transcripts, major players in the mucosal inflammatory response, were downregulated the most in Ent001-treated intestinal cell subsets, thus paralleling the molecular

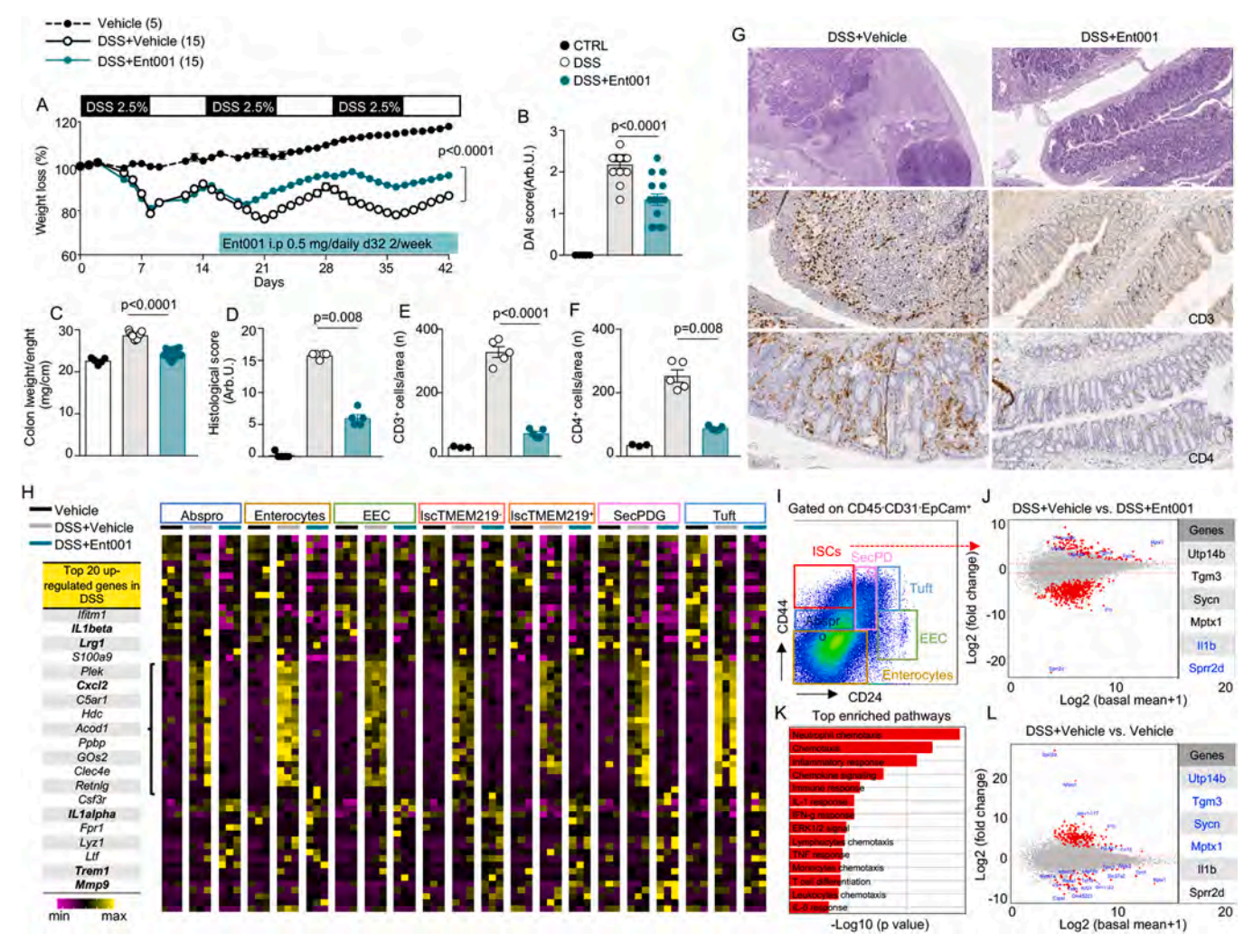


Fig. 4. TMEM219 pharmacological blockade with anti-TMEM219 mAb improves chronic colitis *in vivo*. (A). Line graphs showing percentage of weight loss measured in B6 mice receiving or not oral DSS (2.0 %), three cycles (days 0–7, 14–21, 28–35), and treated with Ent001 (0.5 mg/day/mouse from day 18 to day 32, then every 3 days from day 35 to day 41) or vehicle (PBS, daily for 15 days) in a curative setting (n = 15 mice/group). (B, C, D). Bar graphs representing disease activity Index (DAI) score, colon length and histological score measured at day 42 in untreated mice (n = 5) and in those receiving DSS plus vehicle or Ent001 as in A (n = 15/group). (E, F, G). Bar graphs and representative pictures of histological analysis, including CD4⁺ and CD8⁺ T cells immunostaining, in colon samples of control mice, and in colon of mice receiving DSS+vehicle or DSS+ Ent001. Original magnification 10X, scale bar 200 μm. (H). Heatmap showing the top 20 up-regulated genes in a RNAsequencing analysis performed on flow-sorted intestinal cells subpopulations (enterocytes, ISCs, absorptive and secretory progenitors, enteroendocrine cells and Tufts cells) isolated from crypts of control untreated mice and from DSS+vehicle and DSS+Ent001. In yellow genes expressed the most. (I). Flow plot showing the gating strategy employed to select and flow-sort intestinal cell subsets subjected to RNA seq analysis. (J, K, L). Volcano plots showing up- and down-regulated genes found in the RNAseq analysis compared in mice receiving DSS+vehicle vs. DSS+Ent001 (J) and DSS+vehicle and vehicle (L). On the right in both J and L, a list of genes with p < 0.05 is reported, with downregulated genes in blue. In K, a bar graph represents the top enriched signaling pathways found in J. Data are expressed as mean ± standard error of the mean (SEM) unless otherwise reported. Two-way ANOVA was used in A. One-way ANOVA followed by Sidak's post-hoc test was used in B, C, D, E, and F. Abbreviations: Ent001, anti-TMEM219 monoclonal antibody; DAI, disease activi

profile of naïve animals in whom colitis was not induced (Figs. 4H-I, 4L). Moreover, the increased expression of markers associated to loss of mucosal barrier integrity (*Lrg1*, *Mmp9*) and to bacterial migration/activity (*Clec4e*, *Lyz1*) observed in colitis, was reduced with anti-TMEM219 treatment. These data confirm that administration of the anti-TMEM219 mAb Ent001 suppresses chronic colitis and promotes a healing of the colonic mucosa.

2.7. The anti-TMEM219 mAb Ent001 abrogates inflammatory-mediated carcinogenesis in vivo

Given that chronic inflammation is often associated with carcinogenesis and that this represents a frequent complication in patients with inflammatory bowel disease, we finally tested Ent001 in the inflammatory-mediated carcinogenesis model. This model is also useful to prove whether IGFBP3/TMEM219 blockade with Ent001 is associated with an inflammatory-mediated proliferative effect with the potential development of hyperplastic processes in response to the death cell inhibition. Azomethane (AOM) was injected first at day 0 to induce carcinogenesis, and DSS was chronically administered in three subsequent cycles as described above, with mice receiving anti-TMEM219 mAb Ent001 from day 18 until day 32 daily and then twice a week until the end of the study. Blockade of TMEM219 signal with Ent001 was associated with an improvement in weight loss, DAI and histological score, and a recovery in colon size (Fig. 5A-D). In both non-inflammatory and inflammatory areas, treatment with Ent001 did not

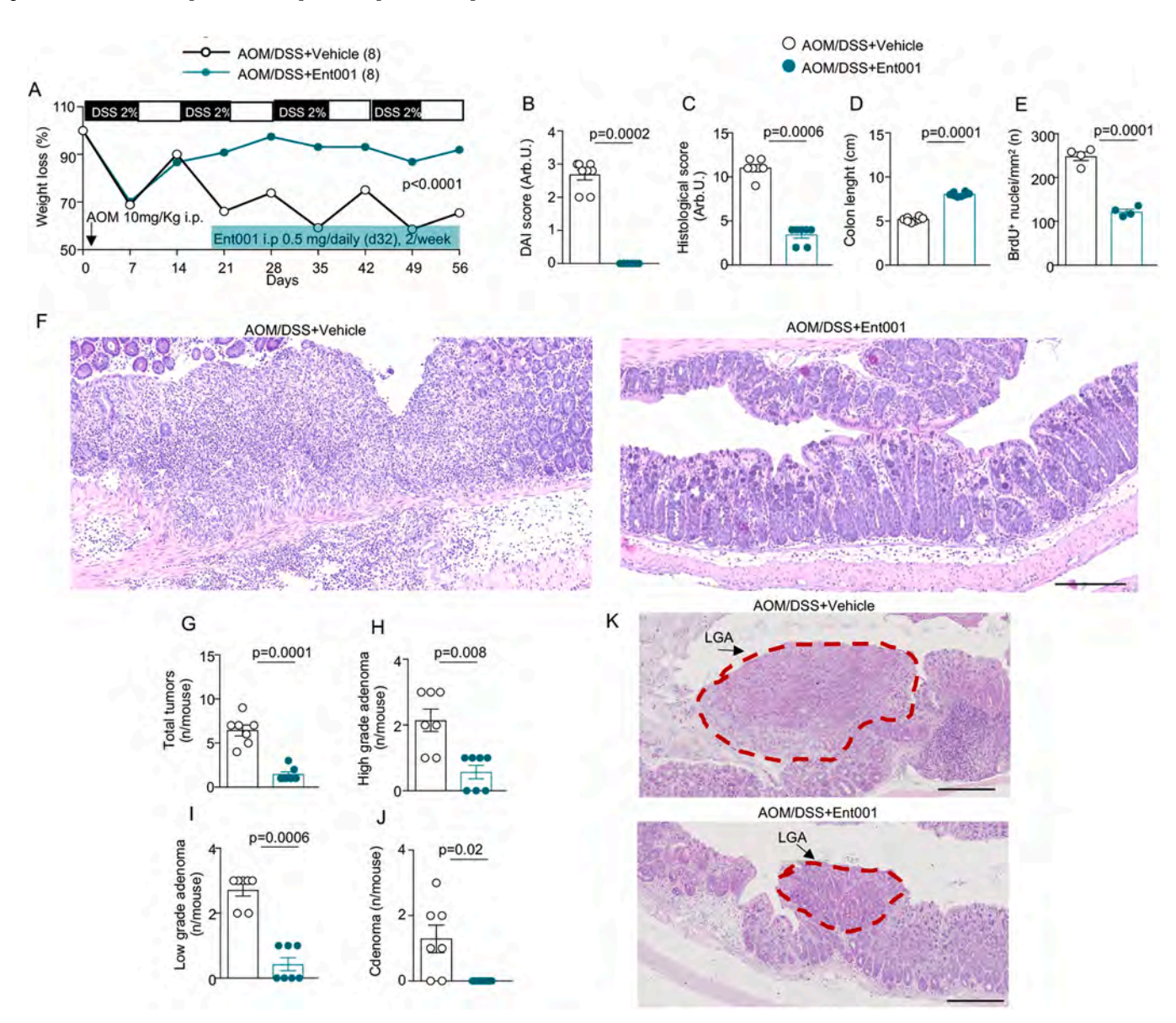


Fig. 5. TMEM219 pharmacological blockade with anti-TMEM219 mAb abrogates inflammatory-mediated carcinogenesis *in vivo*. (A). Line graphs depicting percentage of weight loss measured in B6 mice receiving or not an intraperitoneal AOM injection plus oral DSS (2 %), four cycles (days 0–7, 14–21, 28–35, 42–49), and treated with Ent001 (0.5 mg/day/mouse from day 18 to day 32, then every 3 days from day 35 to day 56) or vehicle (PBS, daily for 15 days) in a curative setting (n = 8 mice/group). (B, C, D, E). Bar graphs representing DAI score, colon length, histological score and BrdU⁺ nuclei per mm² measured at day 56 in mice receiving AOM+DSS plus vehicle or Ent001 as in A (n = 8/group). (F). Representative pictures of histological analysis, in colon samples of mice receiving AOM+DSS+vehicle or AOM+DSS+ Ent001. Original magnification 10X, scale bar 200 μm. (G, H, I, J). Bar graphs representing total number of tumors detected per mouse (G), high-grade adenomas (H), low-grade adenomas (I) and carcinomas (J) quantified in mice receiving AOM+DSS+vehicle or AOM+DSS+Ent001. (K). Representative pictures of low-grade adenomas size in mice receiving AOM+DSS+vehicle or AOM+DSS+Ent001. Original magnification 20X, scale bar 100 μm. Data are expressed as mean ± standard error of the mean (SEM) unless otherwise reported. Two-way ANOVA was used in A. Two-sided t test was used in B, C, D, E, G, H, I and J. Abbreviations: Ent001, anti-TMEM219 monoclonal antibody Ent001; DAI, disease activity index; DSS, dextran sulfate sodium; AOM, azomethane; Arb, arbitrary.

affect epithelial cell proliferation, with a lower number of BrdU⁺ cells measured in the colon sections as compared to AOM+DSS vehicle-treated mice (Fig. 5E). A reduction in infiltrating inflammatory cells with a recovery in crypts morphology was also evident in Ent001-treated mice, and it was associated with a decrease in the number/density of tumors developed (Fig. 5F-G). With regard to the type of tumor, a remarkable decrease in the number and size of low-grade and high-grade adenomas was documented in mice treated with Ent001, while carcinomas did not develop (Fig. 5H-K). These findings demonstrate an improvement of inflammatory-mediated carcinogenesis upon TMEM219 blockade in the intestinal mucosa with no acceleration in tumor initiation/development and further establish that direct blockade of TMEM219 with an anti-TMEM219 antibody such as Ent001 is not associated with any pro-carcinogenic or hyperproliferative effect in chronic colitis.

3. Discussion

In this study we screened and characterize novel therapeutic agents aimed at targeting the IGFBP3/TMEM219 axis in human disease conditions with a particular focus on immune-mediated gastrointestinal disease. While our previous studies used some recombinant proteins as functional inhibitors of the axis [16], in this study we moved to generate monoclonal antibodies, as these are compounds well-tolerated, with a high rate of efficient production and successful results in clinical trials [17-20]. As the technology to produce mAbs has faced significant advancements in the last decades [21], we employed two major strategies. First, we generated fully humanized mAbs by using a phage display approach, widely used nowadays, but appearing in the market just recently and with still some pitfalls to be fixed [22]. The method is however very quick and yield both a good amount of compound and a good number of candidates to be tested and screened in in vitro and in vivo assays [22,23]. The second approach we employed is a more traditional one, the use of a hybridoma-based production, which consists of injecting the antigen of interest in a transgenic mouse that further starts to produce human IgG against it [24,25]. We employed two different strategies also in selecting our disease target. Indeed, we generated monoclonal antibodies against the ligand, IGFBP3, and the receptor, TMEM219. This allowed us to screen an adequate number of candidates and select the most appropriate one in targeted assays. Our in vitro studies demonstrated that both anti-TMEM219 and anti-IGFBP3 mAbs, regardless of the technique used to generate them, possessed beneficial effects in preventing ISCs dysfunction and preserve the ability to develop *in vitro* mini-guts, thereby suggesting their use as promising in intestinal diseases in which regeneration may be disrupted (e.g., diabetic enteropathy). Of note, hybridoma-based mAbs appeared less effective in rescuing organoids development in presence of IGFBP3, maybe due to binding to a different epitope. However, we decided not to directly target IGFBP3, as this may cause a displacement of IGF-1, a growth factor involved in several biological and relevant processes, with an alteration in its availability and function. Therefore, we moved to select our clinical candidate among the anti-TMEM219 mAbs. We are aware that targeting a receptor may also have some drawbacks, such as the fact that a receptor may be expressed in other cells and tissues [26]. In our case, however, blockade of the pathway will occur only in conditions in which the axis is dysregulated, such as diabetic enteropathy and immune-mediated intestinal disorders, thereby avoiding to target a mechanism active in physiological conditions. To this aim, we specifically selected antibodies that showed a KD of 10^{-8} to obtain high efficacy without perturbing the host's immune system. Moreover, TMEM219 expression has been documented in few tissues and the IGFBP3/TMEM219 apoptotic signaling has been demonstrated in few target cells [5,14,15]. Once the mAbs against IGFBP3 were excluded, the analyses conducted on the remaining anti-TMEM219 mAbs, the phage display TC01 and the hybridoma-based TM1, identified TC01 as the lead candidate to move forward to tailored in vivo studies and clinical trials.

Even though the majority of mAbs is still produced by hybridomas [27–30], phage display is now considered the best tool to screen binding sites between receptor and ligands [31-33], such as IGFBP3 and TMEM219, and thus it may perfectly fit in our scenario. Indeed, some mAbs generated by phage display are being quite successful in the treatment of the target disease, with 14 being approved by FDA and among those the TNF/TNFR inhibitor Adalimumab immune-mediated diseases or the PD1/PDL1 inhibitor Atezolizumab for bladder cancer [34]. This may support our strategy of selecting a lead candidate screened by phage display to better target a specific ligand-receptor signaling, allowing us to proceed with the clinical development of the anti-TMEM219 blocking mAb Ent001. To this aim, we successfully tested the anti-TMEM219 blocking mAb Ent001 in in vivo preclinical strategic models, the inflammatory chronic colitis with significant translational potentials in the treatment of inflammatory bowel disease and the inflammatory-related carcinogenesis for potential hyperproliferative effects. Treatment with Ent001 suppressed chronic colitis and promoted mucosal healing, with some remarkable anti-inflammatory effects. This is most likely due to an indirect effect that Ent001 has in blocking cell death and thus preventing that negative signals may be generated outright, thus triggering local inflammation and favoring the recruitment of immune cells. This result was also supported in the inflammatory-mediated carcinogenesis model, in which Ent001 also showed no pro-carcinogenic effects in the mucosa. The ability of Ent001 of primarily acting in promoting the healing of the mucosa by protecting its self-renewal abilities suggest also the potentials of combining this approach with current anti-inflammatory strategies available (e.g., anti-TNF-alpha mAb), to maximize both the regenerative and anti-inflammatory effects. Notably, novel compounds that target the IL23 pathway, a4b7 integrin, or JAK in IBD are emerging [35] and may be also employed in combination with Ent001, having all different therapeutic targets. Interestingly, our previous data showing that TMEM219 blockade was effective in rescuing diabetic enteropathy [14], may further suggest testing Ent001 also in other gastro-intestinal diseases [13]. One limitation of our study is that we would need to identify which biomarker may predict responsiveness to Ent001 treatment. We may speculate that reduction of intestinal ISC markers (LGR5, EPHB2) or upregulation of CASP8 may represent tissue markers to be considered in combination with some peripheral inflammatory factors. Indeed, data on combination therapies studies and identification of biomarkers associated with response to Ent001 treatment are important to proceed with the clinical development of Ent001. A limitation to the generalizability of the study is also that it did not consider gender/sex issues. In summary, we have delineated here a novel potential clinical candidate, with strong evidence in vitro and in vivo, to be considered as a novel therapeutic option in immune-mediated and inflammatory bowel disease.

4. Methods

4.1. Generation of mAbs from naïve human phage-display libraries

Monoclonal anti-TMEM219 and anti-IGFBP3 antibodies were selected from naïve human phage-display libraries using human ectoT-MEM219 (obtained from Genescript's customized protein service) or recombinant human IGFBP3 (R&D Systems, 675-B3) as antigens for the screening, respectively. The ecto-TMEM219 antigen was immobilized onto 96-well ELISA plates either by direct adsorption or capturing via an anti-TMEM219 polyclonal antibody. After washing and blocking of the wells with BSA, the antibody-phage libraries were added. The libraries were cleared from sticky or cross-reactive antibody-phage previously. The phage that displayed an antigen-specific antibody were captured on the plate surface. After removal of unbound/weakly bound phage by washing with PBS-T, antigen-specific phage was eluted and amplified. This amplified library subset was again selected for target binding by increasing the number of washing steps to clear non-bound or weakly

bound phage. In total, three selection rounds were performed to enrich antigen specific antibody-phage. At the end of the selection process, the selection output was screened for antigen-specific antibodies by ELISA. For this purpose, monoclonal scFv antibodies were produced from clones of the selection output. These were then tested for specific antigen binding by ELISA. 15 target specific hits were identified. 11 of them contained a unique CDR sequence. These were cloned into a mammalian scFv-Fc expression vector, resulting in a genetic fusion of the scFv with a human IgG4 Fc. 6 of those antibodies could be produced in the scFv-Fc format by transient transfection of HEK293 cells. The antibodies were purified by affinity chromatography (Protein A) and re-buffered in PBS. The protein concentration was determined by UV/VIS spectrometry and purity was checked by Coomassie staining. The purity of the samples was finally confirmed by using SDS-PAGE with a sample volume of 1 ug loaded to the gel.

4.2. Competitive ELISA binding assay

In order to test anti-IGFBP3 and anti-TMEM219 monoclonal antibodies we employed an ELISA and used IGFBP3 (R&D System) and ecto-TMEM219-his tagged recombinant protein (GenScript's). CVC microplates were coated with 50 µl/well of 4 µg/ml rhIGFBP3 dissolved in PBS or PBS alone (no coating). Plates were incubated 90 min at 37°C and washed with PBS (300 µl/well) and incubated with the blocking reagent (200 μ l/well) 2 h at room temperature. Samples were then diluted in the diluent solution (50 μ l/well) and added to the plate as following: diluent solution (none), ecto-TMEM219 10 µg/ml, ecto-TMEM219 10 µg/ml + anti-IGFBP3 or anti-TMEM219 mAbs 10 μg/ml, anti-IGFBP3 or anti-TMEM219 mAbs 10 µg/ml alone. After washing steps, plates were then incubated at room temperature for 1 h with anti 6X His tag HRP diluted 1:2000 in Diluent solution (50 μ l/well). ELISA plate was then read after adding visualization solution at ELISA reader. The absorbance measured the His tag signal. Ecto-TMEM219 was used as positive control.

4.3. Human studies

Intestinal bioptic and serum samples were obtained from patients with/without Crohn's disease (n = 15/group) who underwent coloscopy within the routinely clinical practice, matched for age (patients with Crohn's disease 46.0 ± 1.0 years old, patients without Crohn's disease 45.0 ± 2.0 years old) and gender (all males), with duration of disease in patients being 14.0 ± 1.0 years. This study was conducted in accordance with the ethics committee Milano Area 1 approval (Stem Cells IBD protocol, n. 2017/ST/277) and a written consent was obtained. As healthy subjects, patients without inflammation who were admitted for other diagnostic reasons were included. All studies were conducted in compliance with all relevant ethical regulations for studies involving human subjects. The study conforms to recognized ethical standards of the Declaration of Helsinki. Human tissues were procured in line with WHO Guiding Principles on Human Cell, Tissue and Organ Transplantation.

4.4. In vitro studies

4.4.1. Isolation of crypts and mini-guts assay

Crypts were isolated from human bioptic colonic samples as previously reported [14,36]. Colon tissue was incubated with mixed antibiotics, cut and incubated in PBS supplemented with 10 mM Dithiothreitol (DTT) (Sigma). EDTA (8 mM) was added to tissue for 30 min at 37° C and crypts were collected from the supernatant, mixed with Matrigel and plated on pre-warmed culture dishes. After solidification of Matrigel, crypts were covered with medium containing Wnt3a-conditioned medium and Advanced DMEM/F12 (Life Technologies, 50:50 ratio), supplemented with 10 mM Nicotinamide, 50 ng/ml human EGF (Life Technologies), 1 µg/ml RSPO1 (Sino Biological), Glutamax (Sigma),

10 mM HEPES, N-2 [1X], B-27 without retinoic acid [1 \times], 1 mM N-Acetyl-L-cysteine, 100 ng/ml human Noggin (Peprotech), 1 µg/ml Gastrin (Sigma- Aldrich), 500 nM LY2157299 (Axon MedChem), 10 µM SB202190 (Sigma) and 0.01 µM PGE2 (Sigma). Every 3 days medium was changed [37]. Mini-guts developing at least 1 crypt domain at 8 days after culture were counted. Percentage of development was calculated based on mini-guts counted at day + 1 and developed at day + 8. Pictures of mini-guts were acquired with Axio Vision AC Release 4.3 at an inverted microscope Leica. Pictures reported in figures represent mini-guts at day 8, 10X magnification.

4.4.2. qRT-PCR analysis

RNA was extracted from samples using TRIzol Reagent (Invitrogen, Carlsbad, CA), reverse-transcribed using Super Script II Reverse Transcriptase (Invitrogen) and quantitative reverse transcriptase polymerase chain reaction (qRT-PCR) analysis was performed in duplicates using TaqMan assays (Life Technologies). Data obtained were normalized for the expression of ACTB, and $\Delta\Delta$ Ct (fold change) was calculated. The primers used for human genes are reported below:

Gene Symbol	Refseq Accession #	Band Size (bp)	Reference Position
LGR5	NM_003667	91	1665
EPHB2	NM_004442	68	2908
CASP8	NM 001080124.1	124	648
ACTB	NM_001101	174	730

4.4.3. Protein interventional studies

Recombinant human IGFBP3 (R&D Systems, 8874-B3, 50 ng/ml) and newly generated anti-IGFBP3 or anti-TMEM219 mAbs (10 $\mu g/ml$, 40:1 ratio to IGFBP3) were added to mini-guts cultures at day + 1. Pooled sera were obtained from at least n=5 patients with long-term Crohn's disease (14.0 \pm 1.0 years of duration, males, aged 46.0 \pm 1.0 years old) and added to culture 10 % in place of regular Fetal bovine serum (FBS) as already described [14].

4.4.4. Ent001 model generation

The Ent001 antibody was modelled using a locally installed version of ColabFold [38]. Ent001 sequence (corresponding to the heavy and light chains) was used as input and modelled as a heterodimer using three recycles. To better shape the model as a full-IgG antibody, the crystal structure of a neutralizing human IgG (PDB ID: 1HZH) was used as a template. Using Coot [39], the Fc portion of the Ent001 model was separated from the Fab portion by the flexible hinge (ranging from 219 to 233 of the heavy chain). Fc and Fab were superposed to the respective portions of the 1HZH model and re-connected through the flexible hinge. To generate the full model of Ent001, with two identical heavy chains and two identical light chains, a copy of the obtained model was then generated and superposed to the second half of the 1HZH model through the Fc portion. The four chains were finally merged into a single PDB file.

4.5. In vivo studies

4.5.1. Animal studies

C57Bl/6 N (B6) mice aged 7 weeks were purchased from Charles River Laboratories (#632, SAS France). Animals had free access to standard mouse chow and tap water and were housed three to five per cage. All the procedures in mice conformed to the Italian law on animal care (D.L. 26/2014), as well as the European Directive (2010/63/UE), and animal experimentation was approved by the Italian Ministry of Health (n. 1144/2020-PR).

4.5.2. DSS chronic colitis model

In the chronic colitis model 7-weeks-old C57Bl/6 N mice were treated with three oral cycles of 2 % DSS (40 kda; MP Biomedicals), with

5 days of DSS exposure in drinking water, followed by 7 days of regular drinking water. Anti-TMEM219 mAb Ent001 was injected intraperitoneally 18 days after starting the DSS treatment at a dose of 0.5/mg/mouse daily from day 18 to day 32, then every 3 days from day 35 to day 41. As vehicle control PBS was injected. Animals were sacrificed at day 42 and colons were collected for *ex vivo* evaluation.

4.5.3. Inflammatory-mediated carcinogenesis colitis model

7-weeks-old C57Bl/6 N mice received a single intraperitoneal injection of Azoxymethane (AOM, 10 mg/Kg), and were treated with repeated oral cycles of 2 % DSS, each characterized by 7 days of DSS exposure in drinking water, followed by 7 days of regular water. The anti-TMEM219 mAb Ent001 was administered at 0.5 mg/mouse intraperitoneally daily from day 18 to day 32, then twice a week until day 56. Colitis severity was assessed through the DAI score based on daily evaluation of body weight, stool consistency, and presence of blood in the stools. At day 56, colons were excised and collected to perform measurement of colon length, histological analysis on formalin-fixed paraffin sections, tumor density, grade and size.

4.5.4. Clinical assessment of colitis in animal models

Colitis severity was monitored using a disease activity index (DAI) score based on daily evaluation of body weight, stool consistency, and presence of blood in the stools, as determined using Hemoccult SENSA Cards (Beckman Coulter); grading of intestinal inflammation was determined according to the criteria already proposed [40]; the DAI has been determined by scoring changes in: weight loss (0 = none, 1 = 1 %–5 %, 2 = 5 %–10 %, 3 = 10 %–20 %, 4 = >20 %); stool consistency (0 = normal, 2 = loose, 4 = diarrhea); and rectal bleeding (0 = normal, 2 = occult bleeding, 4 = gross bleeding). A 5-point (0–4) DAI was thus obtained. Percentage of body weight loss was also calculated as an independent clinical parameter. At the end of the experiment (day 42), animals were euthanized by carbon dioxide (CO2) and colons excised and collected to perform measurement of colon length and weight, histological analysis, qualitative and quantitative evaluation of T cells infiltrating the colon.

4.5.5. Flow sorting

To collect single cell for RNA sequencing analysis isolation of crypts and cells was performed as following. Briefly, upon cutting into 5-10 small pieces, each colon was collected in 5 ml of Trypsin/DNAse solution [DNase, 100 U/ml (Merckmillipore) and Tryple Express Trypsin 1X (Thermofisher Scientific)] at 37°C for 20 min under slow rotation. After washing in PBS, the pieces were then passed through a 100-um cell strainer and incubated for additional 20 min at 37 $^{\circ}\text{C}$ under slow rotation in a 50 ml tube. After an additional washing in PBS, LPMCs end epithelial cells were carefully collected and resuspended immediately in FACS buffer (HBSS 2 % FCS). Cells were stained with the following antibodies: EF450 anti-CD45 (48-0451-82, Thermofisher) to exclude leukocytes, 645 anti-CD31 (47-0112-80, Thermofisher) to exclude endothelial cells, PE-Cy7 anti-EpCAM (25-5791-80, Thermofisher) to positively select intestinal epithelial cells, PE anti-CD24 (12-0242-82, Thermofisher), superbright 702 anti-CD44 (67-0441-82, Thermofisher) and APC-EFluor 780 anti-CD117 (Enthera) to positively select different crypt cells population, including absorptive and secretory progenitors, enterocytes, tuft cells and enteroendocrine cells.

4.5.6. RNAsequencing analysis

RNA from sorted cells was extracted with the RNeasy Plus Universal Mini Kit (Qiagen) and resuspended nuclease free water. RNA quantity and purity were determined with Nanodrop; RNA integrity was measured with Agilent 2100, and RNA integrity number (RIN) was calculated. Reverse transcription and cDNA amplification were performed with the SMARTseq® HT kit (Takara). Libraries were constructed using the Illumina Nextera XT kit and analyzed for concentration (Qubit DNA assay and NanoDrop; Thermo Fisher

Scientific), size distribution (Agilent Bioanalyzer) and quantification of viable sequencing templates via qPCR. Sequencing was performed on the Illumina HiSeq 2500 in Rapid Run Mode with 2×150 bp paired-end configuration. Bioinformatic analysis was conducted by Genewiz and Syneos Health. Sequencing reads were first assessed for overall quality. Hence, sequence reads were trimmed to remove possible adapter sequences and nucleotides with poor quality using Trimmomatic v.0.36. The trimmed reads were mapped to the Mus musculus GRCm38 reference genome available on ENSEMBL using the STAR aligner v.2.5.2b. The STAR aligner is a splice aligner that detects splice junctions and incorporates them to help align the entire read sequences. BAM files were thus generated. Unique gene hit counts were calculated by using feature Counts from the Subread package v.1.5.2. The hit counts were summarized and reported using the gene id feature in the annotation file. Only unique reads that fell within exon regions were counted. After extraction of gene hit counts, the gene hit counts table was used for downstream differential expression analysis. Using DESeq2, a comparison of gene expression between the customer-defined groups of samples was performed. The Wald test was used to generate p-values and log2 fold changes. Genes with an adjusted p-value < 0.05 and absolute log2 fold change > 1 were identified as differentially expressed genes for each comparison. A gene ontology analysis was performed on the statistically significant set of genes by implementing the software GeneSCF v.1.1-p2. The mgi GO list was used to cluster the set of genes based on their biological processes and determine their statistical significance. A list of genes clustered based on their gene ontologies was generated. To evaluate the expression levels of alternatively spliced transcripts, the splice variant hit counts were extracted from the RNA-seq reads mapped to the genome. Differentially spliced genes were identified for groups with more than one sample by testing for significant differences in read counts on exons (and junctions) of the genes using DEXSeq. For groups with only one sample, the exon hit count tables were provided. Statistical analyses were performed using GraphPad Prism 7 (GraphPad Software) using one-way ordinary ANOVA with Dunnett's multiple comparisons test. Data were presented as means \pm SEM and differences were considered statistically significant when p < 0.05

4.5.7. Statistical analysis

Continuous variables are reported as means with standard errors and compared by using two-sided t-tests (Student's t test or Mann-Whitney for data with or without normal distribution respectively). For multiple comparisons, one-way or two-way ANOVA followed by Tukey and/or Sidak post hoc test between the group of interest and all other groups were used, while Kruskal-Wallis analysis was employed in the presence of multiple nonparametric data. Two-tailed P values of less than 0.05 were considered statistically significant. All the analyses were performed with GraphPad Prism V7.

CRediT authorship contribution statement

Stefano Porzio: Methodology, Investigation, Formal analysis. Maria Gabriella Camboni: Methodology, Investigation, Funding acquisition. Anna Maestroni: Methodology, Investigation, Formal analysis. Fiorina Paolo: Writing - review & editing, Supervision, Funding acquisition, Conceptualization. Monique Zangarini: Methodology, Formal analysis, Data curation. Emma Assi: Visualization, Formal analysis, Data curation. Adriana Petrazzuolo: Methodology, Investigation, Data curation. Cristian Loretelli: Validation, Supervision, Methodology, Investigation. Ahmed Abdelsalam: Methodology, Data curation. Andy Joe Seelam: Validation, Methodology. Moufida Ben Nasr: Visualization, Validation, Supervision, Methodology. Vera Usuelli: Methodology, Investigation, Data curation. Virna Marin: Validation, Supervision, Funding acquisition, Formal analysis. Chiara Bruckmann: Visualization, Methodology, Investigation, Formal analysis. Monica Zocchi: Methodology, Investigation, Data curation. Domenico Corradi: Validation, Supervision, Formal analysis. Filippo Canducci: Writing -

review & editing, Supervision, Investigation, Funding acquisition. Claudia Nardini: Supervision, Resources, Project administration, Funding acquisition. Marta Nardini: Validation, Methodology, Formal analysis, Data curation. Giovanni Amabile: Funding acquisition, Data curation, Conceptualization. Sampietro Gianluca M: Writing - review & editing, Validation, Supervision. D'Addio Francesca: Writing original draft, Visualization, Formal analysis, Data curation, Conceptualization. Sandro Ardizzone: Writing – review & editing, Validation, Supervision. Silvio Danese: Validation, Supervision. Gianvincenzo Zuccotti: Writing - review & editing, Validation, Supervision.

Disclosure

P.F. and F.D'A. hold a patent on IGFBP3/TMEM219 axis. G.A., P.F. and F.D. hold equity in Enthera S.r.l. G.A., V.M., C.B., M.N., S.P., M.Z., F. C. and C.N. are/were employees of Enthera S.r.l. S.A is a member of the Enthera Clinical Advisory Board. The other authors have nothing to disclose.

Acknowledgments and Funding

We thank the "Fondazione Romeo e Enrica Invernizzi" for extraordinary support. F.D'A. is supported by Italian Ministry of Health grant RF-2021-12372897 and by the Italian Ministry of University and Research grant 2022JY9CPX. P.F., C.L. and M.BN. are supported by the Italian Ministry of University Research grant 20229ZA2YF, 2022NH9MXB, 20225HWJMB respectively. We thank Enthera for supplying the drugs tested and for contributing to the research design.

Declaration of Competing Interest

The authors declare the following financial interests/personal relationships which may be considered as potential competing interests: P. F. and F.D. hold a patent on IGFBP3/TMEM219 axis. G.A., P.F. and F.D. hold equity in Enthera S.r.l. G.A., V.M., C.B., M.N., S.P., M.Z., F.C. and C. N. are/were employees of Enthera S.r.l. S.A is a member of the Enthera Clinical Advisory Board. The other authors have nothing to disclose. Given his role as Associate Editor of Pharmacological Research, PF had no involvement in the peer-review of this article, and no access to information regarding its peer-review. Full responsibility for the editorial process for this article was delegated to another journal editor".

Appendix A. Supporting information

Supplementary data associated with this article can be found in the online version at doi:10.1016/j.phrs.2025.107901.

Data Availability

Data will be made available on request.

References

- [1] R.C. Baxter, Insulin-like growth factor binding protein-3 (IGFBP-3): novel ligands mediate unexpected functions, J. Cell Commun. Signal 7 (3) (2013) 179-189.
- [2] R.C. Baxter, Insulin-like growth factor binding proteins in the human circulation: a eview, Horm. Res 42 (4-5) (1994) 140-144.
- [3] D.R. Clemmons, Modifying IGF1 activity: an approach to treat endocrine disorders, atherosclerosis and cancer, Nat. Rev. Drug Discov. 6 (10) (2007) 821–833.

 [4] B.E. Forbes, A.J. Blyth, J.M. Wit, Disorders of IGFs and IGF-1R signaling pathways,
- Mol. Cell Endocrinol, 518 (2020) 111035.
- [5] Q. Cai, M. Dozmorov, Y. Oh, IGFBP-3/IGFBP-3 receptor system as an Anti-Tumor and Anti-Metastatic signaling in cancer, Cells 9 (5) (2020).
- [6] A.R. Ingermann, Y.F. Yang, J. Han, A. Mikami, A.E. Garza, L. Mohanraj, L. Fan, M. Idowu, J.L. Ware, H.S. Kim, D.Y. Lee, Y. Oh, Identification of a novel cell death receptor mediating IGFBP-3-induced anti-tumor effects in breast and prostate cancer, J. Biol. Chem. 285 (39) (2010) 30233-30246.
- [7] Y. Oh, Z. Gucev, L. Ng, H.L. Muller, R.G. Rosenfeld, Antiproliferative actions of insulin-like growth factor binding protein (IGFBP)-3 in human breast cancer cells, Prog. Growth Factor Res 6 (2-4) (1995) 503-512.

- [8] Y.C. Lee, S. Jogie-Brahim, D.Y. Lee, J. Han, A. Harada, L.J. Murphy, Y. Oh, Insulinlike growth factor-binding protein-3 (IGFBP-3) blocks the effects of asthma by negatively regulating NF-kappaB signaling through IGFBP-3R-mediated activation of caspases, J. Biol. Chem. 286 (20) (2011) 17898-17909.
- [9] S. Jogie-Brahim, D. Feldman, Y. Oh, Unraveling insulin-like growth factor binding protein-3 actions in human disease, Endocr. Rev. 30 (5) (2009) 417-437.
- J.V. Silha, P.C. Sheppard, S. Mishra, Y. Gui, J. Schwartz, J.G. Dodd, L.J. Murphy, Insulin-like growth factor (IGF) binding protein-3 attenuates prostate tumor growth by IGF-dependent and IGF-independent mechanisms, Endocrinology 147 (5) (2006) 2112–2121.
- [11] S. Joyce, A.M. Nour, Blocking transmembrane219 protein signaling inhibits autophagy and restores normal cell death, PLoS One 14 (6) (2019) e0218091.
- [12] R.C. Baxter, Signalling pathways involved in antiproliferative effects of IGFBP-3: a review, Mol. Pathol. 54 (3) (2001) 145-148.
- [13] F. D'Addio, P. Fiorina, Type 1 diabetes and dysfunctional intestinal homeostasis, Trends Endocrinol. Metab. 27 (7) (2016) 493-503.
- [14] F. D'Addio, S. La Rosa, A. Maestroni, P. Jung, E. Orsenigo, M. Ben Nasr, S. Tezza, R. Bassi, G. Finzi, A. Marando, A. Vergani, R. Frego, L. Albarello, A. Andolfo, R. Manuguerra, E. Viale, C. Staudacher, D. Corradi, E. Batlle, D. Breault, A. Secchi, F. Folli, P. Fiorina, Circulating IGF-I and IGFBP3 levels control human colonic stem cell function and are disrupted in diabetic enteropathy, Cell Stem Cell 17 (4) (2015) 486-498.
- [15] F. D'Addio, A. Maestroni, E. Assi, M. Ben Nasr, G. Amabile, V. Usuelli, C. Loretelli, F. Bertuzzi, B. Antonioli, F. Cardarelli, B. El Essawy, A. Solini, I.C. Gerling, C. Bianchi, G. Becchi, S. Mazzucchelli, D. Corradi, G.P. Fadini, D. Foschi, J F. Markmann, E. Orsi, J. Skrha Jr., M.G. Camboni, R. Abdi, A.M. James Shapiro, F. Folli, J. Ludvigsson, S. Del Prato, G. Zuccotti, P. Fiorina, The IGFBP3/TMEM219 pathway regulates beta cell homeostasis, Nat. Commun. 13 (1) (2022) 684.
- [16] F. D'Addio, G. Amabile, E. Assi, A. Maestroni, A. Petrazzuolo, C. Loretelli, A. Abdelasalam, M. Ben Nasr, I. Pastore, M.E. Lunati, V. Usuelli, M. Zocchi, A. J. Seelam, D. Corradi, S. La Rosa, V. Marin, M. Zangarini, M. Nardini, S. Porzio, F. Canducci, C. Nardini, B. El Essawy, M. Nebuloni, J. Yang, M. Venturini, G. Maconi, F. Folli, S. Danese, G. Zuccotti, G.M. Sampietro, S. Ardizzone, P. Fiorina, TMEM219 signaling promotes intestinal stem cell death and exacerbates colitis, J. Clin. Invest 135 (10) (2025).
- [17] A.C. Chan, P.J. Carter, Therapeutic antibodies for autoimmunity and inflammation, Nat. Rev. Immunol, 10 (5) (2010) 301-316.
- [18] A.L. Nelson, E. Dhimolea, J.M. Reichert, Development trends for human monoclonal antibody therapeutics, Nat. Rev. Drug Discov. 9 (10) (2010) 767-774.
- [19] N.A. Buss, S.J. Henderson, M. McFarlane, J.M. Shenton, L. de Haan, Monoclonal antibody therapeutics: history and future, Curr. Opin. Pharm. 12 (5) (2012) 615-622.
- [20] F.C. Breedveld, Therapeutic monoclonal antibodies, Lancet 355 (9205) (2000) 735-740.
- [21] A. Mullard, 2018 FDA drug approvals, Nat. Rev. Drug Discov. 18 (2) (2019) 85–89.
 [22] T. Jostock, M. Vanhove, E. Brepoels, R. Van Gool, M. Daukandt, A. Wehnert, R. Van Hegelsom, D. Dransfield, D. Sexton, M. Devlin, A. Ley, Hoogenboom H. Mullberg, J. Rapid generation of functional human IgG antibodies derived from Fab-on-phage display libraries, J. Immunol. Methods 289 (1-2) (2004) 65-80.
- [23] T.J. Vaughan, A.J. Williams, K. Pritchard, J.K. Osbourn, A.R. Pope, J.C. Earnshaw, J. McCafferty, R.A. Hodits, J. Wilton, K.S. Johnson, Human antibodies with subnanomolar affinities isolated from a large non-immunized phage display library, Nat. Biotechnol. 14 (3) (1996) 309-314.
- [24] N. Lonberg, Fully human antibodies from transgenic mouse and phage display platforms, Curr. Opin. Immunol. 20 (4) (2008) 450-459.
- [25] L.L. Green, M.C. Hardy, C.E. Maynard-Currie, H. Tsuda, D.M. Louie, M.J. Mendez, H. Abderrahim, M. Noguchi, D.H. Smith, Y. Zeng, N.E. David, H. Sasai, D. Garza, D. G. Brenner, J.F. Hales, R.P. McGuinness, D.J. Capon, S. Klapholz, A. Jakobovits, Antigen-specific human monoclonal antibodies from mice engineered with human ig heavy and light chain YACs, Nat. Genet 7 (1) (1994) 13-21.
- [26] R. Santos, O. Ursu, A. Gaulton, A.P. Bento, R.S. Donadi, C.G. Bologa, A. Karlsson, B. Al-Lazikani, A. Hersey, T.I. Oprea, J.P. Overington, A comprehensive map of molecular drug targets, Nat. Rev. Drug Discov. 16 (1) (2017) 19-34.
- [27] G. Kohler, C. Milstein, Continuous cultures of fused cells secreting antibody of predefined specificity, Nature 256 (5517) (1975) 495-497.
- [28] A.S. Andre, I. Moutinho, J.N.R. Dias, F. Aires-da-Silva, In vivo phage display: a promising selection strategy for the improvement of antibody targeting and drug delivery properties, Front Microbiol 13 (2022) 962124.
- [29] Aires da Silva, F. Santa-Marta, M. Freitas-Vieira, A. Mascarenhas, P. Barahona, I. Moniz-Pereira, J. Gabuzda, D. Goncalves, J. Camelized rabbit-derived VH singledomain intrabodies against vif strongly neutralize HIV-1 infectivity, J. Mol. Biol. 340 (3) (2004) 525–542.
- [30] F. Aires da Silva, S. Corte-Real, J. Goncalves, Recombinant antibodies as therapeutic agents: pathways for modeling new biodrugs, BioDrugs 22 (5) (2008)
- Y. Tan, T. Tian, W. Liu, Z. Zhu, C JY. Advance in phage display technology for bioanalysis, Biotechnol. J. 11 (6) (2016) 732-745.
- [32] J. Babickova, L. Tothova, P. Boor, P. Celec, In vivo phage display-a discovery tool in molecular biomedicine, Biotechnol. Adv. 31 (8) (2013) 1247-1259.
- J. Greenwood, A.E. Willis, R.N. Perham, Multiple display of foreign peptides on a filamentous bacteriophage. Peptides from Plasmodium falciparum circumsporozoite protein as antigens, J. Mol. Biol. 220 (4) (1991) 821–827.
- M.A. Alfaleh, H.O. Alsaab, A.B. Mahmoud, A.A. Alkayyal, M.L. Jones, S.M. Mahler, A.M. Hashem, Phage display derived monoclonal antibodies: from bench to bedside, Front Immunol. 11 (2020) 1986.

- [35] S. Honap, V. Jairath, S. Danese, L. Peyrin-Biroulet, Navigating the complexities of drug development for inflammatory bowel disease, Nat. Rev. Drug Discov. 23 (7) (2024) 546–562.
- [36] P. Jung, T. Sato, A. Merlos-Suarez, F.M. Barriga, M. Iglesias, D. Rossell, H. Auer, M. Gallardo, M.A. Blasco, E. Sancho, H. Clevers, E. Batlle, Isolation and in vitro expansion of human colonic stem cells, Nat. Med. 17 (10) (2011) 1225–1227.
- [37] T. Sato, H. Clevers, Growing self-organizing mini-guts from a single intestinal stem cell: mechanism and applications, Science 340 (6137) (2013) 1190–1194.
- [38] M. Mirdita, K. Schutze, Y. Moriwaki, L. Heo, S. Ovchinnikov, M. Steinegger, ColabFold: making protein folding accessible to all, Nat. Methods 19 (6) (2022) 679–682.
- [39] P. Emsley, B. Lohkamp, W.G. Scott, K. Cowtan, Features and development of coot, Acta Crystallogr D. Biol. Crystallogr 66 (Pt 4) (2010) 486–501.
- [40] S. D'Alessio, C. Correale, C. Tacconi, A. Gandelli, G. Pietrogrande, S. Vetrano, M. Genua, V. Arena, A. Spinelli, L. Peyrin-Biroulet, C. Fiocchi, S. Danese, VEGF-C-dependent stimulation of lymphatic function ameliorates experimental inflammatory bowel disease, J. Clin. Invest. 124 (9) (2014) 3863–3878.